nature genetics

Titin-truncating variants affect heart function in disease cohorts and the general population

Sebastian Schafer[1,2,17], Antonio de Marvao[3,17], Eleonora Adami[4], Lorna R Fiedler[2], Benjamin Ng[1], Ester Khin[2], Owen J L Rackham[2], Sebastiaan van Heesch[4], Chee J Pua[1], Miao Kui[2], Roddy Walsh[5], Upasana Tayal[5], Sanjay K Prasad[5], Timothy J W Dawes[3], Nicole S J Ko[2], David Sim[1], Laura L H Chan[1], Calvin W L Chin[1,2], Francesco Mazzarotto[5], Paul J Barton[5], Franziska Kreuchwig[4], Dominique P V de Kleijn[6,7], Teresa Totman[6], Carlo Biffi[3], Nicole Tee[1], Daniel Rueckert[8], Valentin Schneider[4], Allison Faber[4], Vera Regitz-Zagrosek[9,10], Jonathan G Seidman[11], Christine E Seidman[11–13], Wolfgang A Linke[14,15], Jean-Paul Kovalik[2], Declan O'Regan[3], James S Ware[3,5,18], Norbert Hubner[4,10,16,18] & Stuart A Cook[1,2,5,18]

Titin-truncating variants (TTNtv) commonly cause dilated cardiomyopathy (DCM). TTNtv are also encountered in ~1% of the general population, where they may be silent, perhaps reflecting allelic factors. To better understand TTNtv, we integrated *TTN* allelic series, cardiac imaging and genomic data in humans and studied rat models with disparate TTNtv. In patients with DCM, TTNtv throughout titin were significantly associated with DCM. Ribosomal profiling in rat showed the translational footprint of premature stop codons in *Ttn*, TTNtv-position-independent nonsense-mediated degradation of the mutant allele and a signature of perturbed cardiac metabolism. Heart physiology in rats with TTNtv was unremarkable at baseline but became impaired during cardiac stress. In healthy humans, machine-learning-based analysis of high-resolution cardiac imaging showed TTNtv to be associated with eccentric cardiac remodeling. These data show that TTNtv have molecular and physiological effects on the heart across species, with a continuum of expressivity in health and disease.

DCM has a prevalence of up to 1:250 (ref. 1), is the most common indication for heart transplantation and is often associated with TTNtv (15–20% of DCM cases), which are enriched in the titin A-band[2,3]. A surprising ~1% of the general population has a TTNtv in the absence of DCM, which has stimulated much debate as to the pathogenicity of TTNtv[4–7]. It has been suggested that TTNtv in the healthy population may be phenotypically silent and that TTNtv that segregate in familial DCM are perhaps modifiers of other DCM-causing variants[3]. However, it is also known that variants in disease-linked genes can be associated with quantitative differences in the physiology of healthy individuals[8], and such a possibility has not been formally assessed for TTNtv.

We showed previously that *TTN* exon characteristics are important determinants of TTNtv pathogenicity. Variants encoded in exons that are not spliced into titin isoforms expressed in the heart (non-cardiac exons with percent spliced in (PSI) <15%) are not associated with DCM[3], whereas variants encoded in exons that only incorporate into the N2BA isoform and not the N2B isoform have weak associations with disease. Studies of human induced pluripotent stem cell (iPSC)-derived cardiomyocytes (iPSC-CMs)[9] showed that alternative exon splicing is a major mechanism of reduced penetrance for some I-band TTNtv. When only taking into account TTNtv that are encoded in cardiac exons (PSI > 15%), approximately 0.5% of the general population has a TTNtv that might be expected to cause DCM but does not.

In addition to the complexities surrounding TTNtv penetrance, the molecular mechanisms underlying pathogenesis mediated by TTNtv are uncharacterized. Neither nonsense-mediated mRNA decay (NMD) of the mutated allele, detected by RNA–seq, nor a reduction in the levels of full-length *TTN*, determined by agarose gel analysis, have been demonstrated, which if documented would support a haploinsufficient disease mechanism[3,9,10]. Equally, accumulation of a truncated titin protein is not apparent in human heart samples[3] and is rarely present in iPSC-CMs[9], suggesting that a poison-peptide/dominant-negative mechanism is unlikely.

[1]National Heart Centre Singapore, Singapore. [2]Duke–National University of Singapore, Singapore. [3]Cardiovascular and Metabolic Disorders Program, MRC Clinical Sciences Centre, Faculty of Medicine, Imperial College London, Hammersmith Hospital Campus, London, UK. [4]Cardiovascular and Metabolic Sciences, Max Delbrück Center for Molecular Medicine in the Helmholtz Association (MDC), Berlin, Germany. [5]National Heart and Lung Institute and NIHR Royal Brompton Cardiovascular BRU, Imperial College London, London, UK. [6]Department of Surgery, National University of Singapore, Singapore. [7]Departments of Cardiology and Vascular Surgery, University Medical Center, Utrecht, the Netherlands. [8]Department of Computing, Imperial College London, London, UK. [9]Institute of Gender in Medicine, Charité Universitätsmedizin Berlin, Berlin, Germany. [10]DZHK (German Centre for Cardiovascular Research), partner site Berlin, Berlin, Germany. [11]Department of Genetics, Harvard Medical School, Boston, Massachusetts, USA. [12]Division of Cardiovascular Medicine, Brigham and Women's Hospital, Boston, Massachusetts, USA. [13]Howard Hughes Medical Institute, Chevy Chase, Maryland, USA. [14]Department of Cardiovascular Physiology, Ruhr University Bochum, Bochum, Germany. [15]DZHK (German Centre for Cardiovascular Research), partner site Goettingen, Goettingen, Germany. [16]Charité Universitätsmedizin, Berlin, Germany. [17]These authors contributed equally to this work. [18]These authors jointly supervised this work. Correspondence should be addressed to S.A.C. (stuart.cook@duke-nus.edu.sg).

Received 28 April; accepted 18 October; published online 21 November 2016; doi:10.1038/ng.3719

Here we undertook studies of human patients with DCM, rat models of TTNtv and human volunteers from the general population to better understand TTNtv pathogenicity and molecular effect, with a specific focus on dissecting a hypothesized position-dependent effect on the penetrance of TTNtv alleles. To do this, we performed a meta-analysis of TTNtv in patients with DCM (n = 2,495) as compared to controls (n = 61,834) and generated two rat models of TTNtv with variants at opposite ends of the titin molecule. We integrated RNA–seq and ribosome profiling (Ribo–seq) data across models and species, and we performed metabolic and signaling studies to outline potential disease mechanisms. To define the effects of TTNtv on the heart in the general population, we sequenced *TTN* in healthy volunteers (n = 1,409) who were deeply phenotyped. We supplemented standard 2D cardiac magnetic resonance imaging (CMR) with high-resolution, high-fidelity 3D CMR, integrating and analyzing the imaging and sequencing data using machine learning techniques.

RESULTS

TTNtv across the titin molecule are associated with DCM

We and others have shown that A-band TTNtv are associated with DCM[2,3,9], but association of TTNtv in the I-band, Z-disc or M-line with DCM has not been demonstrated. It has been suggested that proximal (near N-terminus) TTNtv in particular may be non-penetrant. To investigate variant effects across the titin molecule, we retrieved TTNtv alleles from patients with DCM in available sources, combined these data with those for new DCM cases (n = 1,105) and performed a meta-analysis using the Exome Aggregation Consortium (ExAC) database[11] and other controls (cohort totals: DCM cases, n = 2,495; controls, n = 61,834; Online Methods). This analysis showed that TTNtv encoded in constitutive exons (PSI > 90%) were significantly associated with DCM, irrespective of their position in titin (**Table 1**).

While some I-band TTNtv may be rescued by differential splicing[9], we observed that I-band TTNtv encoded in constitutive cardiac exons were significantly associated with DCM, which was true for both proximal and distal I-band variants. TTNtv in Z-disc-encoding exons were also associated with DCM, although with a much lower odds ratio (OR = 5.3) than was found for A-band TTNtv (OR = 49.8). It has been proposed that a distal internal promoter of the Cronos titin isoform[12], which we confirmed to be present in adult human heart using cap analysis of gene expression (CAGE)[13] data (**Supplementary Fig. 1**), can rescue proximal TTNtv effects. However, we found that proximal TTNtv were also penetrant and associated with DCM. By splitting titin into protein regions (**Table 1**) or consecutive uniformly sized bins (n = 40; **Supplementary Fig. 2**), we were able to show that the fraction of truncating variants that were penetrant (etiological fraction) in regions of titin encoded upstream of the Cronos promoter was comparable to the fraction in the downstream A-band. These data show that distal I-band and all A-band TTNtv have larger odds ratios than very proximal or distal variants, suggesting position-dependent effects on the penetrance of TTNtv in DCM.

Premature stop codons cause nonsense-mediated mRNA decay and disrupt translation of full-length, sarcomere-spanning titin

Our meta-analyses of patients with DCM showed that TTNtv throughout the titin molecule are penetrant but have variable, position-related odds ratios. To study putative position-dependent effects in greater detail while controlling for other genetic and non-genetic factors, we modeled proximal and distal TTNtv in two independent rat strains on the same genetic background (TTNtvA, variation in the A-band; TTNtvZ, variation in the Z-disc; for details, see **Supplementary Fig. 3**). Rats with homozygous mutations were not viable, as previously described for TTNtv in mice[10], while heterozygous rats were born in normal Mendelian ratios (data not shown).

We bred TTNtv heterozygous rats on a F344 background with Brown Norway rats with wild-type *Ttn* to obtain an F_1 cross to enable allele-specific analysis of *Ttn* transcription and translation in the hearts of TTNtvA (n = 3), TTNtvZ (n = 3) and wild-type (n = 4) rats using RNA–seq and Ribo–seq (**Fig. 1a** and **Supplementary Fig. 4**)[14,15]. Ribosome-protected fragments (RPFs) showed clear trinucleotide periodicity across the translatome, indicating the presence of actively translating ribosomes (**Fig. 1b**). *Ttn* transcripts encoding a truncation in the A-band were transcribed and translated as far as the nonsense codon, which efficiently stopped translation thereafter (**Fig. 1c**,**d**).

The premature stop codon of the TTNtvZ allele did not prevent translation downstream of the non-canonical stop codon, and F344 SNPs on the *Ttn* allele encoding the truncation were detected throughout *Ttn* (**Fig. 1e**). Rescue of translation from the truncating F344 allele did not decrease the 3-nt periodicity across *Ttn* in comparison to F_1 wild-type rats that synthesized titin from two intact alleles (**Fig. 1f**). Exon-level analyses showed that the TTNtvZ variant initially reduced ribosome occupancy at the 5′ end of *Ttn* (~50% that of wild-type occupancy), but translation was subsequently partially recovered (**Fig. 1g**). This apparent rescue of translation might be explained in part by internal ribosomal entry sites (IRES), by transcription start sites that generate titin isoforms with alternative N termini, and potentially by factors that maintain ribosomes on the long *Ttn* transcript during its translation. In support of this hypothesis, human CAGE data[13] and analysis of epigenetic marks[16] identified distal *TTN* promoters in human heart (**Supplementary Fig. 1**),

Table 1 Meta-analysis shows an association of TTNtv encoded in constitutive exons throughout titin with DCM

Sarcomere domain affected by variant	DCM positive (n = 2,495)	Control positive (n = 61,834)	DCM prevalence (%)	Control prevalence (%)	OR	OR (max)	OR (min)	EF	P value
A-band (constitutive)	268	149	10.74	0.24	49.8	61.1	40.6	0.98	2.4×10^{-260}
I-band (distal, constitutive, post-Cronos)	9	7	0.36	0.01	32.0	85.9	11.9	0.97	2.5×10^{-9}
I-band (distal, constitutive, pre-Cronos)	18	23	0.72	0.04	19.5	36.2	10.5	0.95	6.6×10^{-15}
I-band (non-constitutive)	6	102	0.24	0.17	1.5	3.3	0.6	0.31	0.46
I-band (proximal, constitutive)	22	29	0.88	0.05	19.0	33.0	10.9	0.95	1.1×10^{-17}
M-band (constitutive)	6	40	0.24	0.07	3.7	8.8	1.6	0.73	0.01
Z-disc (constitutive)	7	33	0.28	0.05	5.3	11.9	2.3	0.81	0.001
Z-disc (non-constitutive)	0	11	0.00	0.02	NA	NA	NA	NA	NA

Exon usage is displayed according to the levels of PSI[17]: constitutive exons are spliced into titin isoforms with an efficiency of at least 90%. P values indicate significant enrichment for TTNtv in DCM (binomial test). OR, odds ratio; EF, etiologic fraction; NA, not applicable.

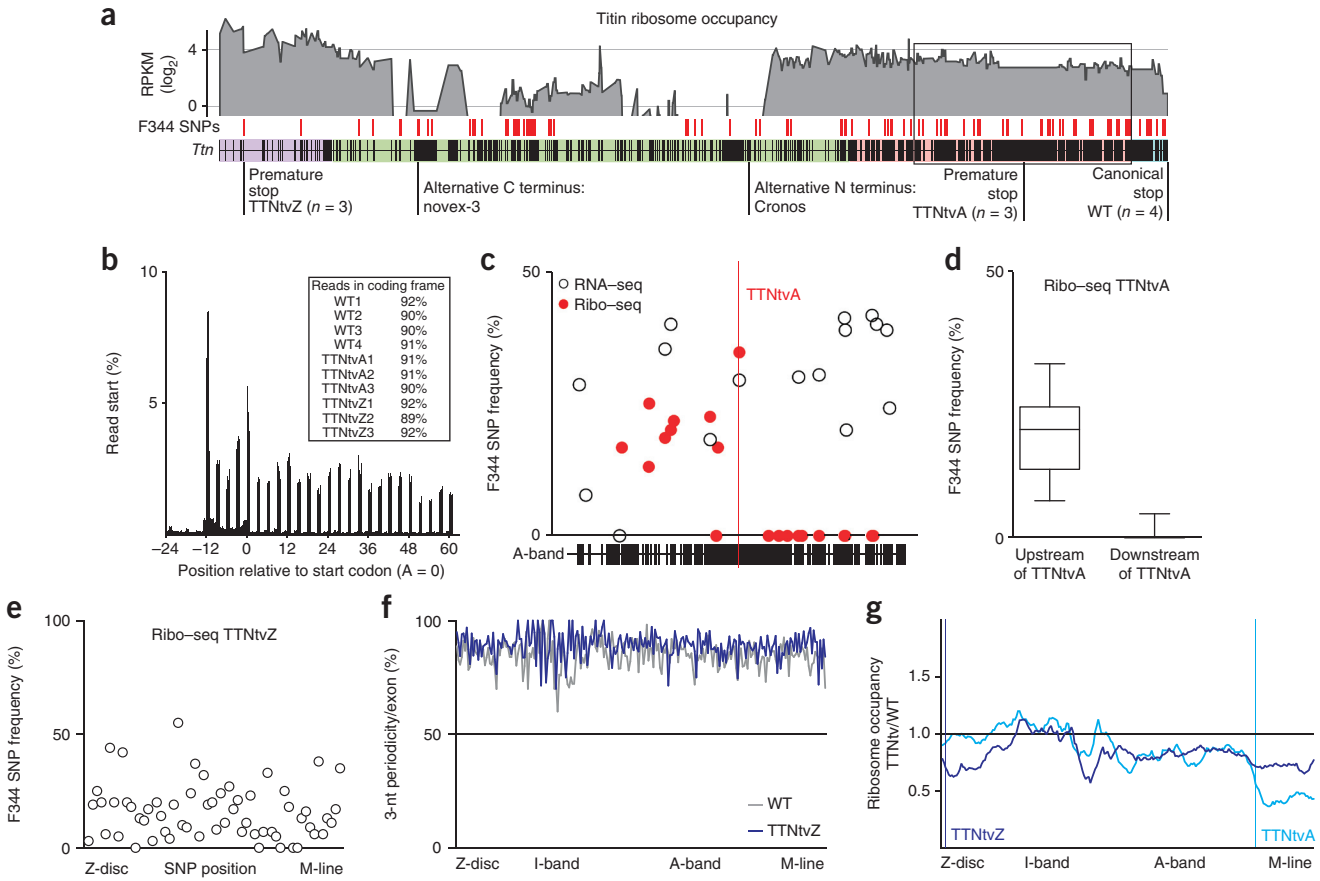

Figure 1 Ribosome profiling identifies the translational footprint of truncating variants in titin. (**a**) Ribosome occupancy across *Ttn*. Average RPKM values are shown per exon for ten BN × F344 F_1 rats. F344 SNPs on the BN background ($n = 121$) allow assessment of allele-specific translation for two distinct models of truncation and rats with wild-type (WT) *Ttn*. Purple, Z-disc; green, I-band; pink, A-band; blue, M-line. (**b**) Ribo–seq reads (28-mers) show clear 3-nt periodicity across the genome for all replicates, indicating that the data sets effectively capture actively translating ribosomes in the heart. (**c**,**d**) Ribosomes occupy the F344 allele in TTNtvA rats upstream of the premature stop codon in the A-band of titin, exposing the synthesis of truncated titin isoforms. (**c**) The premature stop codon releases ribosomes from the mutant *Ttn* message. (**d**) Titin protein synthesized after the TTNtvA premature stop codon is exclusively generated from the intact BN allele. In box plots, boxes show medians within the 25th–75th percentile, and whiskers show the 10th–90th percentile. Allele frequencies in RNA–seq and Ribo–seq data were below 50%, indicative of NMD. (**e**) F344 SNPs located after the TTNtvZ premature stop codon are occupied by ribosomes, indicating translation after the proximal truncating variant in *Ttn*. (**f**) Ribo–seq reads located downstream of the TTNtvZ premature stop codon do not show decreased 3-nt periodicity, suggesting that TTNtvZ rats actively translate canonical *Ttn* sequence at similar levels as rats with two wild-type *Ttn* alleles. (**g**) In TTNtvZ rats, ribosome density is initially reduced, but translation of *Ttn* is gradually rescued. Translation of A-band exons, but not of I-band exons, is reduced in mutants in comparison to wild-type rats. In TTNtvA rats, translation is efficiently reduced after the premature stop codon.

as previously suggested[12]. In TTNtvA rats, we only detected ribosomes on the intact BN allele after the premature stop codon (**Fig. 1c**). This led to a decrease in ribosome occupancy of 50% when compared to wild-type rats that translated this section of *Ttn* from both alleles (**Fig. 1g**).

In both mutant rats, there was a relative increase in the frequency of exon translation in the I-band (**Fig. 1g**) that reflects differential *Ttn* mRNA processing and higher PSI ratios[17] for exons in the I-band, as observed in human iPSC-CMs with TTNtv[9]. This is indicative of an increase in expression of the N2BA isoform in TTNtv carriers. To determine whether this finding would translate to humans, we compared cardiac RNA–seq data[3] from human DCM cases with ($n = 17$) and without ($n = 91$) a TTNtv and observed similar patterns of alternative splicing in TTNtv carriers as were seen in the rat models (**Fig. 2a**). Allele-specific RNA–seq data showed slight upregulation of the wild-type allele and profound NMD of the allele carrying the TTNtv in both the TTNtvA and TTNtvZ models (**Fig. 2b**). These data demonstrate a multiallelic effect of TTNtv on the overall titin isoform composition across species (that can cause DCM[18,19]) and that TTNtv confer position-independent NMD.

It is notable that both the proximal and distal TTNtv triggered NMD with identical efficiency, irrespective of their locations in the titin molecule. The fact that the proximal truncating variant triggers NMD indicates that the premature stop codon close to the 5′ end of the TTNtvZ allele is functional and that ribosomes cannot clear exon–exon junction complexes[20,21]. Assessing translation beyond the truncating variant in the TTNtvA transcript and the four-exon deletion in the TTNtvZ transcript showed that both rat models synthesized lesser amounts (~60% of those in wild-type rats) of full-length, sarcomere-spanning titin (**Fig. 2c**). In keeping with our published data[3], protein gel electrophoresis did not identify a truncated titin isoform or a reduction in the titin/Mhc ratio in mutant rat heart (**Supplementary Fig. 5**). This result suggests rapid turnover of mutant protein that, to our knowledge, we document the existence of for the first time by showing its synthesis (**Fig. 1**). It also shows that, although there are significantly fewer ribosomes translating full-length protein

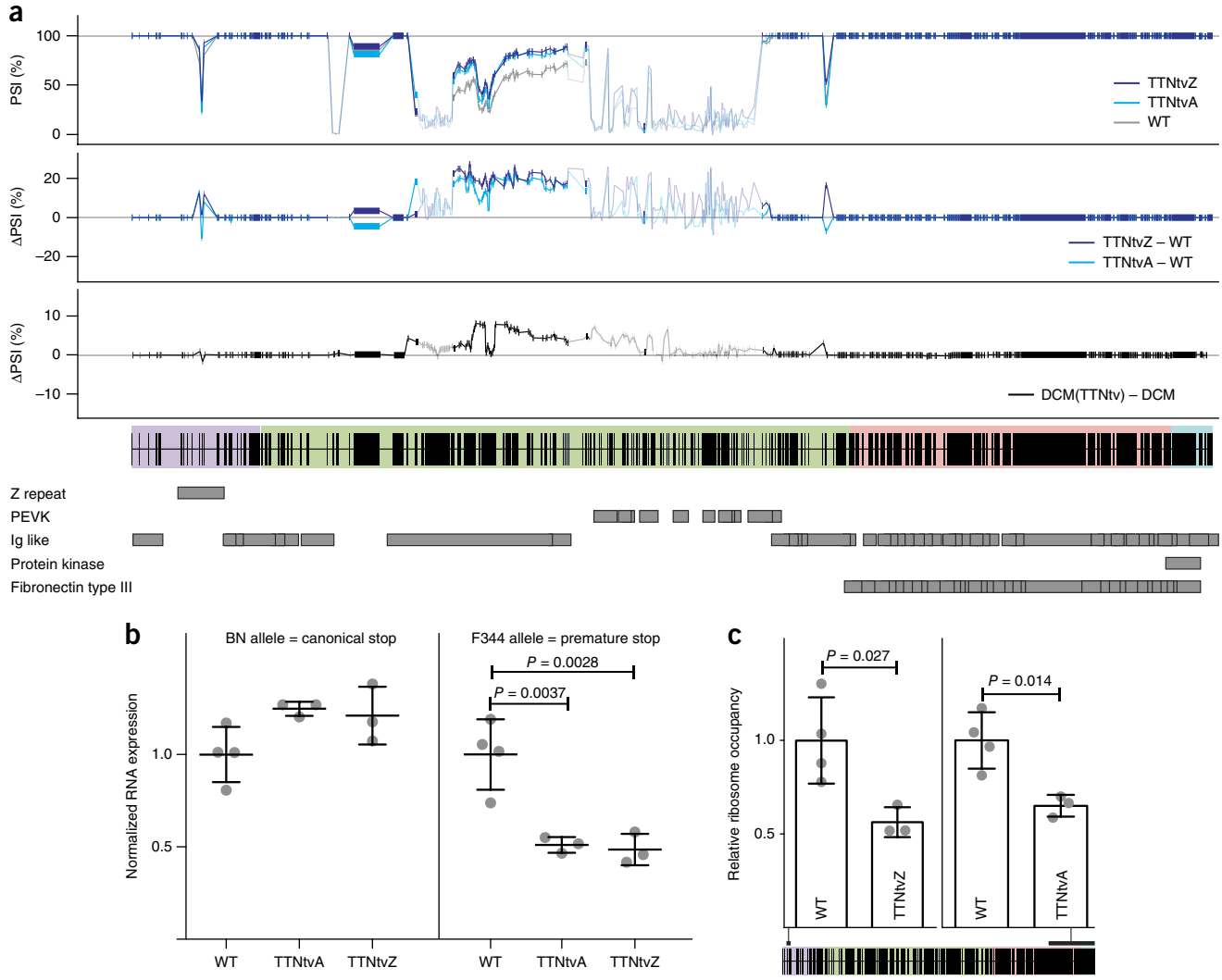

Figure 2 Proximal and distal TTNtv in *Ttn* alter isoform processing and trigger NMD. (**a**) PSI and ΔPSI of *Ttn* exons expressed in the heart for TTNtvA, TTNtvZ and wild-type rats and of *TTN* exons in human DCM cases. Exons with at least ten inclusion reads are shown with solid color. Truncating mutations in *Ttn* activate splicing of I-band exons in the TTNtv rat models, and similar alternative splicing is seen in human patients with DCM who carry truncating mutations in *TTN*. (**b**) RNA–seq reads assigned to either the BN or F344 allele: TTNtv selectively trigger NMD of *Ttn* transcripts encoding truncated protein. Data are shown as means ± s.d.; *P* values were obtained by Dunnett's test. (**c**) Ribo–seq expression of exons that are exclusively synthesized in TTNtvA and TTNtvZ rats shows that both TTNtv models generate 60% of full-length titin in comparison to wild-type rats. Levels of translation are for full-length titin. Data are shown as means ± s.d.; *P* values were obtained by Student's *t* test. Purple, Z-disc; green, I-band; pink, A-band; blue, M-line.

in the mutants (TTNtvA: $P = 0.014$; TTNtvZ: $P = 0.027$), changes in titin protein levels are not apparent at the resolution of gel analysis. Overall changes in the levels of full-length titin protein might be compensated for not just by upregulation of the wild-type allele ($P = 0.02$; **Fig. 2b**) but also via an increase in ribosome translational speed or changes in protein turnover.

Taken together, these data indicate that proximal and distal TTNtv disrupt titin protein synthesis but have different translational footprints. However, the effects of these variants on NMD of the transcripts encoding sarcomere-spanning titin isoforms are similar, leading to identical reductions in the expression of full-length titin.

Titin truncations cause position-independent perturbation of cardiac metabolism and signaling

To determine whether distinct molecular phenotypes are associated with proximal and distal TTNtv, we performed pathway analysis[22] of the genome-wide transcription (RNA–seq) and translation (Ribo–seq) profiles for the TTNtvZ and TTNtvA mutants as compared to controls. The gene expression differences observed between TTNtv rats and wild-type controls were highly correlated for TTNtvA and TTNtvZ, both for the RNA–seq and Ribo–seq data, showing that the mutant strains have similarly perturbed transcriptomes ($R^2 = 0.841$, $P < 0.0001$) and translatomes ($R^2 = 0.837$, $P < 0.0001$; **Supplementary Fig. 6** and **Supplementary Table 1**). Gene set enrichment analyses showed significantly overlapping Kyoto Encyclopedia of Genes and Genomes (KEGG)[22,23] terms for TTNtv rats when compared to wild-type controls (RNA–seq $P < 1 \times 10^{-15}$, Ribo–seq $P < 1 \times 10^{-15}$, Pearson χ^2 test; **Fig. 3a**), which suggests altered cardiac metabolism independent of the positions of the TTNtv.

To investigate further the molecular signatures of altered cardiac metabolism in mutant rats, we performed quantitative metabolomic profiling of hearts from wild-type and TTNtv rats. Liquid

chromatography coupled with mass spectrometry (LC–MS) showed reduced amounts of medium- and long-chain fatty acid acylcarnitines in hearts from TTNtv rats as compared to controls (**Fig. 3b** and **Supplementary Table 2**). We also performed capillary electrophoresis coupled with mass spectrometry, which is complementary to LC–MS, and observed accumulation of alternative myocardial substrates (branched-chain amino acid metabolites and glycolytic intermediates) in mutants (**Fig. 3c–e**, **Supplementary Fig. 7** and **Supplementary Table 3**). These changes are similar to those seen in the failing heart and the pressure-loaded non-failing heart[24,25] and are associated with a shift in cardiac metabolism away from fatty acids and toward glycolysis, which may be adaptive[26–28]. There was no change in the amounts of major energy substrates (for example, ATP; **Supplementary Fig. 8**), which are only diminished in advanced cardiac failure[29].

The signaling changes in the heart due to TTNtv are likely many. We found that variations in the amounts of metabolic proteins that interact with titin, such as Fhl2 (**Supplementary Fig. 9**), were small, and the functional roles of these changes cannot be established on the

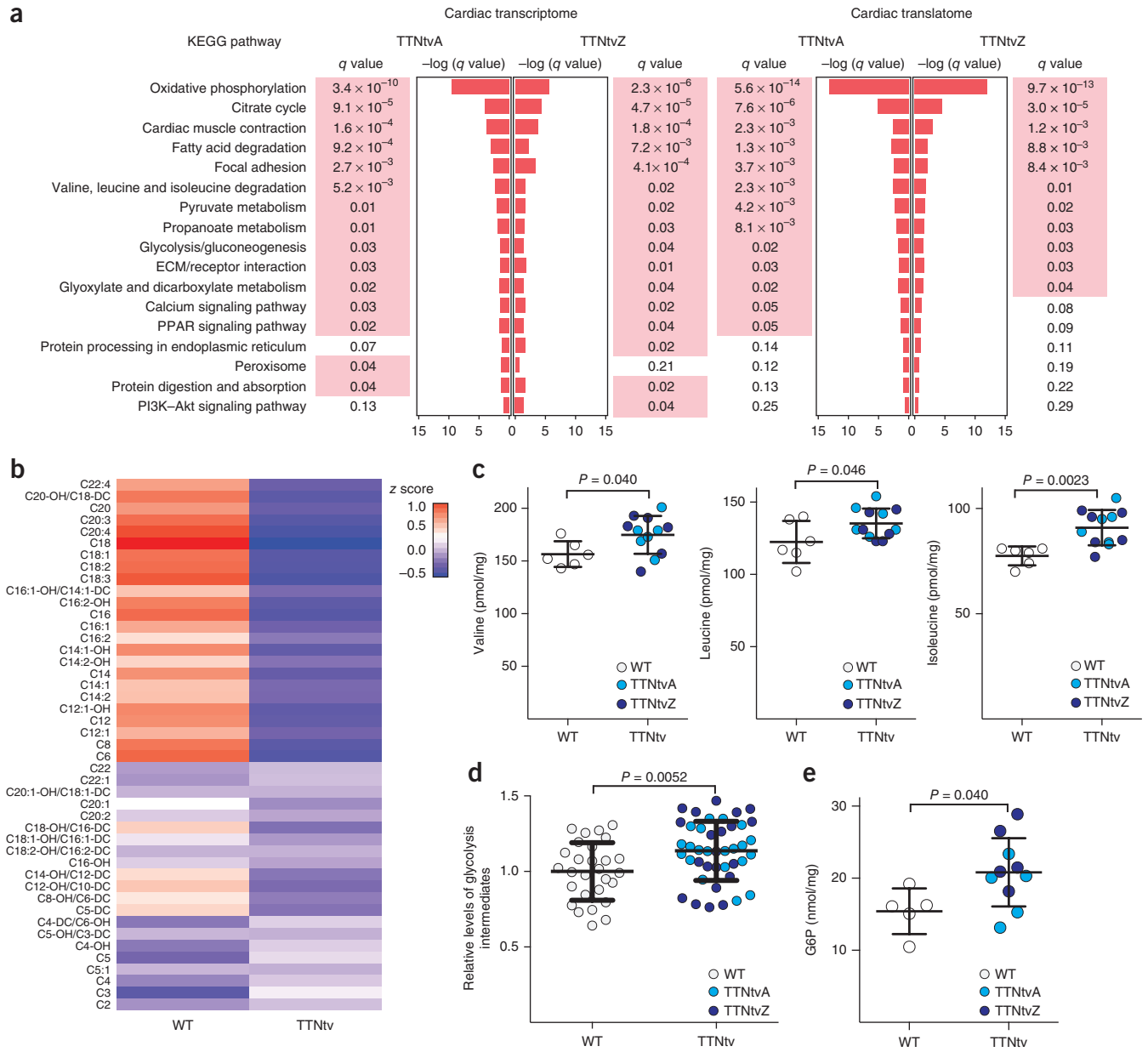

Figure 3 Hearts with proximal and distal truncations of titin undergo metabolic reprogramming. (**a**) Pathway analyses based on RNA–seq and Ribo–seq data suggest perturbed metabolism, structural integrity and mechanosensation in TTNtv heart. This molecular signature is strikingly similar in rats with proximal and distal truncations ($P < 1 \times 10^{-15}$, Pearson χ^2 test). Significantly enriched pathways are highlighted in red (corrected $P < 0.05$). (**b**) Unsupervised clustering of cardiac acylcarnitines by abundance in wild-type ($n = 5$) and TTNtv ($n = 10$) rats using *k*-means clustering. *z* score denotes distance from mean in multiples of s.d. "OH" and "DC" designate hydroxylated and dicarboxylic acid acylcarnitine species, respectively. (**c**) Metabolite profiles showing the abundance of branched-chain amino acids (valine, leucine and isoleucine). Data are shown as means ± s.d.; *P* values were obtained by Student's *t* test. (**d**) Sum of measured levels for glycolytic intermediates (metabolites are detailed in **Supplementary Table 3**). Data are shown as means ± s.d.; the *P* value was obtained by Student's *t* test. (**e**) Glucose-6-phosphate (G6P) amounts in cardiac tissue from wild-type ($n = 6$) and TTNtv ($n = 12$) rats. Data are shown as means ± s.d.; the *P* value was calculated by Student's *t* test. For results for individual genotypes (wild-type versus TTNtvA or TTNtvZ), see **Supplementary Figure 7**.

basis of these data alone. It is known that mTORC1 signaling is activated in familial DCM[30], and the activity of this pathway is detrimental in a mouse model of DCM due to *Lmna* mutation[31]. We profiled the mTORC1 pathway in hearts from TTNtv rats, where the levels of metabolites activating mTOR[32] were elevated (**Fig. 3**), and observed activation of signaling (**Supplementary Fig. 10**). The relative importance of such signaling variation for DCM pathobiology remains to be established.

TTNtv impair cardiac performance during stress in rats and have adverse effects on the heart in the general human population

In young TTNtv rats (<8 months old), cardiac imaging showed features of concentric remodeling but normal left ventricle mass and systolic function (**Supplementary Fig. 11**). In older rats (>1 year old), TTNtv hearts were similar to controls, although with a suggestion of slightly impaired systolic function (**Fig. 4a** and **Supplementary Fig. 12**).

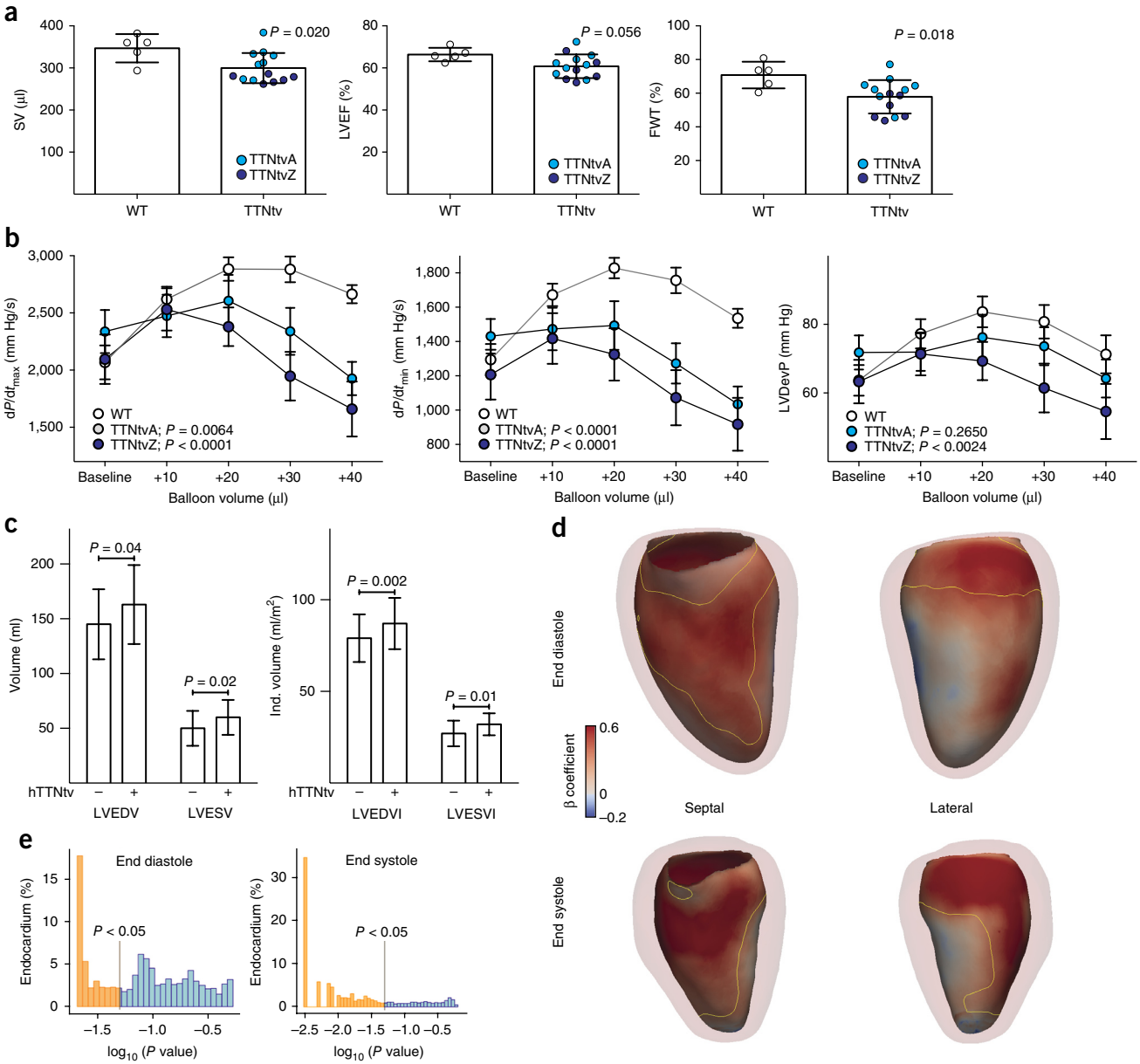

Figure 4 TTNtv in rats and humans adversely affect cardiac geometry and function. (**a**) SV (stroke volume), LVEF (left ventricle ejection fraction) and FWT (fractional wall thickening) measured with CMR in 13- to 16-month-old male wild-type ($n = 5$) and TTNtv (TTNtvA, $n = 8$; TTNtvZ, $n = 6$) rats. Data are shown as means ± s.d.; *P* values were obtained by Student's *t* test. For individual genotypes, see **Supplementary Figure 12**. (**b**) Measurements of *ex vivo* myocardial function during volume overload stress in 4-month-old wild-type ($n = 9$) and TTNtv (TTNtvA, $n = 8$; TTNtvZ, $n = 8$) rats. TTNtv hearts have mildly increased myocardial contraction rate (dP/dt_{max}), myocardial relaxation rate (dP/dt_{min}) and left ventricle developed pressure (LVDevP) at baseline. Data are shown as means ± s.e.m.; *P* values were obtained by two-way ANOVA. (**c**–**e**) Human data. (**c**) Univariate analyses of left ventricular end diastolic volume (LVEDV), LVEDV indexed to body surface area (LVEDVI), left ventricular end systolic volume (LVESV) and LVESV indexed to body surface area (LVESVI). Healthy human individuals without a TTNtv ($hTTNtv^-$) are compared to healthy humans with a TTNtv ($hTTNtv^+$). Data are shown as means ± s.d.; *P* values were obtained by Mann–Whitney test. (**d**) Computational modeling of cardiac geometry in healthy humans using 3D CMR. Positive standardized *β* coefficients indicate where TTNtv status is associated with enlargement of the left ventricle cavity at end diastole and end systole. Septal and lateral *en face* projections are shown with an outline of the left ventricle myocardium. The area enclosed by the yellow contour has corrected $P < 0.05$ (mass univariate linear regression). (**e**) Distribution of corrected *P* values as a proportion of the endocardial surface (mass univariate linear regression).

Although changes in cardiac morphology and function were mild in young mutant rats, it is possible that this phenotype represents a compensated state, as evidenced by the shift in cardiac metabolism (**Fig. 3**), which is adaptive, at least in the short term[26]. We examined cardiac function *ex vivo* and used a volume overload model to test Frank–Starling response, which may specifically be impaired by genetic variation in *TTN*[33]. Under basal conditions (left ventricle end diastolic pressure of 5–10 mm Hg), rat hearts harboring TTNtv tended to have higher strain rates and left ventricle developed pressures, perhaps reflecting compensatory metabolism (**Fig. 3**) and signaling (**Supplementary Fig. 10**); however, when hearts were subjected to stress from sequential volume overload, mutant heart function became increasingly impaired (**Fig. 4b**). As observed previously[34–36], cardiac stress *ex vivo* activated mTORC1 signaling in control rats, which is an adaptive response. However, hearts harboring TTNtv had elevated mTORC1 signaling at baseline and were not able to appropriately increase mTORC1 activity further when stressed (**Supplementary Fig. 10**).

In rat, TTNtv had mild effects on heart function irrespective of their positions in the titin molecule but did not cause DCM. To explore the possibility that TTNtv in cardiac exons similarly affect the heart in human subjects, irrespective of disease status, we recruited 1,409 healthy individuals for detailed CMR studies of the heart in combination with *TTN* sequencing. We specifically focused our studies on the cardiac parameters of left ventricle end diastolic volume (LVEDV) and ejection fraction (EF), which are used to define DCM[37], and also left ventricle end systolic volume (LVESV), which is elevated in pre-DCM cases and predicts the onset of heart failure[38]. In this cohort, we identified 15 TTNtv (**Supplementary Table 4**; prevalence = 1.0%) in *TTN* exons (PSI > 15%), in keeping with our previous findings[3] and data from ExAC[11]. Variants resulting in truncation were equally distributed across the titin molecule in our cohort and in the ExAC data set (**Supplementary Fig. 13**).

After genotype-blinded analysis of CMR data, we found that no individual from the general population with a TTNtv met imaging criteria for DCM, similar to our observations in the rat models and previous studies[3]. However, in univariate analyses, TTNtv conferred a significant increase in absolute left ventricle volume and had pronounced effects on volume indexed to body surface area (**Fig. 4c**). There was a non-significant trend toward lower left ventricle ejection fraction in individuals harboring TTNtv (LVEF (%): TTNtv positive, 66 ± 5; TTNtv negative, 63 ± 5; $P = 0.06$, Mann–Whitney test). Given the multiple clinical and anthropometric variables that predict cardiac morphology and function, we built regression models for LVEDV, LVESV and LVEF (Online Methods and **Supplementary Table 5**) and tested whether addition of TTNtv status improved model performance, which turned out to be the case (absolute β values: LVEDV, +11.8 ml (8.1%); LVESV, +7.7 ml (15%); LVEF, −2.8%; $P < 0.03$ for all). Of note, the effect size of TTNtv on cardiac parameters was much greater than the effect sizes of loci identified by cardiovascular genome-wide association studies (GWAS; for example, systolic blood pressure, for which the combined effect of all GWAS-identified loci was ~3%)[39,40].

To complement our 2D studies, we collected an independent data set of high-resolution, single-breath-hold 3D CMR images and, blinded to genotype, performed atlas- and machine-learning-based analyses of left ventricle geometry with respect to TTNtv status[41,42]. The 3D data showed that TTNtv were associated with eccentric cardiac remodeling in healthy individuals. This remodeling was defined by outward displacement of the endocardial border of the heart (**Fig. 4d**,**e** and **Supplementary Video 1**) in both systole (79% of total surface, $P < 0.05$) and diastole (47% of total surface, $P < 0.05$), in consensus with the 2D data showing larger left ventricle volumes at these phases of the cardiac cycle.

DISCUSSION

Here we studied the effects of TTNtv in patients with DCM, in the rat and in healthy humans to better understand these variants that represent the most common genetic cause of DCM, yet are prevalent in the general population. At the molecular level, we found that TTNtv cause altered I-band splicing and position-independent NMD, which attenuates the synthesis of sarcomere-spanning titin isoforms. The NMD of the TTNtv allele that we observed in the F_1 rat cross is, to our knowledge, the first demonstration of this effect and something we were not able to show previously using unphased human RNA–seq data[3]. Distal truncations are associated with synthesis of C-terminally truncated titin isoforms, whereas proximal TTNtv lead to translation of additional titin isoforms with alternative N termini. None of these additional isoforms were detected on protein gels, suggesting that these species are rapidly degraded (**Supplementary Fig. 5**). It was notable that, irrespective of their position in the titin molecule, proximal and distal premature stop codons in rat caused highly similar gene expression and translational signatures. While these molecular phenotypes are sufficient to affect heart function, these findings do not exclude the possibility of additional, position-dependent effects that modify TTNtv penetrance in DCM, where distal I-band and all A-band TTNtv have the highest odds ratios.

The molecular phenotype due to TTNtv, which is reminiscent of cardiac adaptation to heart failure stimuli with a shift away from fatty acid metabolism[26–28], was associated with activation of the mTORC1 pathway, which is also activated in familial DCM[30]. We suggest that the metabolic (**Fig. 3**) and signaling (**Supplementary Fig. 10**) changes in hearts harboring TTNtv represent adaptive mechanisms[26–28] and that the heart is maintained in a compensated state and is therefore inflexible to further stress. This may explain why hemodynamic stress associated with pregnancy or possibly a second genetic factor may uncover TTNtv effects[43]. It will be interesting to see what other environmental triggers for DCM (for example, alcohol intake, viral infection or chemotherapy) combine with TTNtv to cause disease and equally to ascertain why some individuals with TTNtv and an interacting stimulus, such as pregnancy, do not develop disease.

We found that TTNtv in constitutive exons throughout the titin molecule, from the Z-disc to the M-line, are significantly associated with DCM. This has implications for interpretation of TTNtv in patients with DCM, although A-band and distal I-band TTNtv have higher odds ratios than variants in other titin domains, for reasons that remain unclear. In the general population, we show that TTNtv that were previously thought to be of limited consequence[44] are associated with higher left ventricular volume in 2D CMR analyses, which reflects underlying eccentric remodeling that was detected using advanced 3D CMR techniques. These data demonstrate the benefits of combining high-resolution phenotyping and machine-based data analysis for imaging genetic studies of the heart, which we suggest may be applied at scale in large cohorts with cardiac imaging and genetic data, such as the UK Biobank. It is apparent that the magnitude of the effects of TTNtv on cardiac geometry in the general population may be large enough to adversely influence future cardiac events in some individuals, and this requires further study.

We note that TTNtv in exons that are expressed in the heart (PSI > 15%) are present in about 0.5% of individuals across ancestry groups[3,11], and it may be that this variant class is of clinical relevance for up to 35 million people, particularly if they are exposed to additional genetic or environmental cardiac stresses. Future studies that pinpoint those at greatest risk from the interaction between a TTNtv and a secondary trigger, genetic or environmental, are needed to move the field forward.

METHODS

Methods, including statements of data availability and any associated accession codes and references, are available in the online version of the paper.

Note: Any Supplementary Information and Source Data files are available in the online version of the paper.

ACKNOWLEDGMENTS

We thank all the patients and healthy volunteers for taking part in this research and our team of research nurses across the hospital sites. We also thank M. von Frieling-Salewsky for technical support. The research was supported by the MRC Clinical Sciences Centre, UK, to J.S.W., S.A.C., A.d.M. and D.P.O'R., the NIHR Biomedical Research Unit in Cardiovascular Disease at Royal Brompton, the Harefield NHS Foundation Trust and Imperial College London to J.S.W. and S.A.C., the NIHR Imperial Biomedical Research Centre, British Heart Foundation, UK (SP/10/10/28431, PG/12/27/29489) to S.A.C., D.P.O'R. and C.B., the Wellcome Trust, UK (107469/Z/15/Z to J.S.W., 087183/Z/08/Z, 092854/Z/10/Z and WT095908), a Wellcome Trust Fellowship (100211/Z/12/Z and P43579_WMET to T.J.W.D.), Fondation Leducq to J.S.W., the Tanoto Foundation to S.A.C., CORDA, the National Institutes of Health (NHLBI 2R01HL080494 to J.G.S. and C.E.S.), the National Medical Research Council (NMRC) Singapore (CIRG13nov024 and STaR13nov002 to D.P.V.d.K.), the SingHealth Duke–NUS Institute of Precision Medicine, the Rosetrees Trust, the Health Innovation Challenge Fund (HICF-R6-373 to J.S.W.) funding from the Wellcome Trust and the Department of Health, UK, the Howard Hughes Medical Institute, the European Union EURATRANS award (HEALTH-F4-2010-241504 to N.H.), the Helmholtz Alliance ICEMED to N.H., European Union FP7 (CardioNeT-ITN-289600 to F.M.), Deutsche Forschungsgemeinschaft (SFB1002, TPA08 to W.A.L., Forschergruppe 1054 HU 1522/1-1 to N.H. and TP1 to V.R.-Z.), and an EMBO Long-Term Fellowship (ALTF 186-2015 to S.v.H.) and Marie Curie Actions (LTFCOFUND2013, GA-2013-609409 to S.v.H.). This publication includes independent research commissioned by the Health Innovation Challenge Fund (HICF), a parallel funding partnership between the UK Department of Health and the Wellcome Trust. The views expressed in this work are those of the authors and not necessarily those of the UK Department of Health or the Wellcome Trust.

AUTHOR CONTRIBUTIONS

S.A.C. conceived, managed and arranged funding for the project. A.d.M., E.A., L.R.F., B.N., E.K., S.v.H., C.J.P., U.T., S.K.P., T.J.W.D., N.S.J.K., D.S., L.L.H.C., C.W.L.C., P.J.B., D.P.V.d.K., T.T., C.B., N.T., V.R.-Z., J.G.S., C.E.S. and W.A.L. performed experiments and contributed clinical data. S.S., A.d.M., O.J.L.R., M.K., R.W., F.M., F.K., D.R., V.S., A.F., J.-P.K., D.P.O'R., J.S.W., N.H. and S.A.C. performed data analysis and interpretation. S.S., B.N. and S.A.C. prepared the manuscript with input from co-authors.

COMPETING FINANCIAL INTERESTS

The authors declare competing financial interests: details are available in the online version of the paper.

1. Hershberger, R.E., Hedges, D.J. & Morales, A. Dilated cardiomyopathy: the complexity of a diverse genetic architecture. *Nat. Rev. Cardiol.* **10**, 531–547 (2013).
2. Herman, D.S. *et al.* Truncations of titin causing dilated cardiomyopathy. *N. Engl. J. Med.* **366**, 619–628 (2012).
3. Roberts, A.M. *et al.* Integrated allelic, transcriptional, and phenomic dissection of the cardiac effects of titin truncations in health and disease. *Sci. Transl. Med.* **7**, 270ra6 (2015).
4. Norton, N. *et al.* Exome sequencing and genome-wide linkage analysis in 17 families illustrate the complex contribution of TTN truncating variants to dilated cardiomyopathy. *Circ Cardiovasc Genet* **6**, 144–153 (2013).
5. Chauveau, C., Rowell, J. & Ferreiro, A. A rising titan: *TTN* review and mutation update. *Hum. Mutat.* **35**, 1046–1059 (2014).
6. Akinrinade, O., Koskenvuo, J.W. & Alastalo, T.-P. Prevalence of titin truncating variants in general population. *PLoS One* **10**, e0145284 (2015).
7. Akinrinade, O., Alastalo, T.P. & Koskenvuo, J.W. Relevance of truncating titin mutations in dilated cardiomyopathy. *Clinic. Genet.* **90**, 49–54 (2016).
8. Robinson, E.B. *et al.* Genetic risk for autism spectrum disorders and neuropsychiatric variation in the general population. *Nat. Genet.* **48**, 552–555 (2016).
9. Hinson, J.T. *et al.* Titin mutations in iPS cells define sarcomere insufficiency as a cause of dilated cardiomyopathy. *Science* **349**, 982–986 (2015).
10. Gramlich, M. *et al.* Stress-induced dilated cardiomyopathy in a knock-in mouse model mimicking human titin-based disease. *J. Mol. Cell. Cardiol.* **47**, 352–358 (2009).
11. Lek, M. *et al.* Analysis of protein-coding genetic variation in 60,706 humans. *Nature* **536**, 285–291 (2016).
12. Zou, J. *et al.* An internal promoter underlies the difference in disease severity between N- and C-terminal truncation mutations of Titin in zebrafish. *eLife* **4**, e09406 (2015).
13. Forrest, A.R. *et al.* A promoter-level mammalian expression atlas. *Nature* **507**, 462–470 (2014).
14. Ingolia, N.T., Ghaemmaghami, S., Newman, J.R. & Weissman, J.S. Genome-wide analysis *in vivo* of translation with nucleotide resolution using ribosome profiling. *Science* **324**, 218–223 (2009).
15. Schafer, S. *et al.* Translational regulation shapes the molecular landscape of complex disease phenotypes. *Nat. Commun.* **6**, 7200 (2015).
16. Kundaje, A. *et al.* Integrative analysis of 111 reference human epigenomes. *Nature* **518**, 317–330 (2015).
17. Schafer, S. *et al.* Alternative splicing signatures in RNA–seq data: percent spliced in (PSI). *Curr. Protoc. Hum. Genet.* **87**, 11.16.1–11.16.14 (2015).
18. Guo, W. *et al. RBM20*, a gene for hereditary cardiomyopathy, regulates titin splicing. *Nat. Med.* **18**, 766–773 (2012).
19. Maatz, H. *et al.* RNA-binding protein RBM20 represses splicing to orchestrate cardiac pre-mRNA processing. *J. Clin. Invest.* **124**, 3419–3430 (2014).
20. Le Hir, H., Izaurralde, E., Maquat, L.E. & Moore, M.J. The spliceosome deposits multiple proteins 20–24 nucleotides upstream of mRNA exon–exon junctions. *EMBO J.* **19**, 6860–6869 (2000).
21. Le Hir, H., Gatfield, D., Izaurralde, E. & Moore, M.J. The exon–exon junction complex provides a binding platform for factors involved in mRNA export and nonsense-mediated mRNA decay. *EMBO J.* **20**, 4987–4997 (2001).
22. Luo, W., Friedman, M.S., Shedden, K., Hankenson, K.D. & Woolf, P.J. GAGE: generally applicable gene set enrichment for pathway analysis. *BMC Bioinformatics* **10**, 161 (2009).
23. Kanehisa, M. & Goto, S. KEGG: Kyoto Encyclopedia of Genes and Genomes. *Nucleic Acids Res.* **28**, 27–30 (2000).
24. Lai, L. *et al.* Energy metabolic reprogramming in the hypertrophied and early stage failing heart: a multisystems approach. *Circ Heart Fail* **7**, 1022–1031 (2014).
25. Shibayama, J. *et al.* Metabolic remodeling in moderate synchronous versus dyssynchronous pacing-induced heart failure: integrated metabolomics and proteomics study. *PLoS One* **10**, e0118974 (2015).
26. Doenst, T., Nguyen, T.D. & Abel, E.D. Cardiac metabolism in heart failure: implications beyond ATP production. *Circ. Res.* **113**, 709–724 (2013).
27. Stanley, W.C., Recchia, F.A. & Lopaschuk, G.D. Myocardial substrate metabolism in the normal and failing heart. *Physiol. Rev.* **85**, 1093–1129 (2005).
28. Schisler, J.C. *et al.* Cardiac energy dependence on glucose increases metabolites related to glutathione and activates metabolic genes controlled by mechanistic target of rapamycin. *J. Am. Heart Assoc.* **4**, e001136 (2015).
29. Neubauer, S. The failing heart—an engine out of fuel. *N. Engl. J. Med.* **356**, 1140–1151 (2007).
30. Yano, T. *et al.* Clinical impact of myocardial mTORC1 activation in nonischemic dilated cardiomyopathy. *J. Mol. Cell. Cardiol.* **91**, 6–9 (2016).
31. Ramos, F.J. *et al.* Rapamycin reverses elevated mTORC1 signaling in lamin A/C-deficient mice, rescues cardiac and skeletal muscle function, and extends survival. *Sci. Transl. Med.* **4**, 144ra103 (2012).
32. Neishabouri, S.H., Hutson, S.M. & Davoodi, J. Chronic activation of mTOR complex 1 by branched chain amino acids and organ hypertrophy. *Amino Acids* **47**, 1167–1182 (2015).
33. Ait-Mou, Y. *et al.* Titin strain contributes to the Frank–Starling law of the heart by structural rearrangements of both thin- and thick-filament proteins. *Proc. Natl. Acad. Sci. USA* **113**, 2306–2311 (2016).
34. Sen, S. *et al.* Glucose regulation of load-induced mTOR signaling and ER stress in mammalian heart. *J. Am. Heart Assoc.* **2**, e004796 (2013).
35. Shende, P. *et al.* Cardiac raptor ablation impairs adaptive hypertrophy, alters metabolic gene expression, and causes heart failure in mice. *Circulation* **123**, 1073–1082 (2011).
36. Zhang, D. *et al.* MTORC1 regulates cardiac function and myocyte survival through 4E-BP1 inhibition in mice. *J. Clin. Invest.* **120**, 2805–2816 (2010).
37. Mestroni, L. *et al.* Guidelines for the study of familial dilated cardiomyopathies. *Eur. Heart J.* **20**, 93–102 (1999).
38. Vasan, R.S., Larson, M.G., Benjamin, E.J., Evans, J.C. & Levy, D. Left ventricular dilatation and the risk of congestive heart failure in people without myocardial infarction. *N. Engl. J. Med.* **336**, 1350–1355 (1997).
39. Levy, D. *et al.* Genome-wide association study of blood pressure and hypertension. *Nat. Genet.* **41**, 677–687 (2009).
40. Newton-Cheh, C. *et al.* Genome-wide association study identifies eight loci associated with blood pressure. *Nat. Genet.* **41**, 666–676 (2009).
41. de Marvao, A. *et al.* Population-based studies of myocardial hypertrophy: high resolution cardiovascular magnetic resonance atlases improve statistical power. *J. Cardiovasc. Magn. Reson.* **16**, 16 (2014).
42. Bai, W. *et al.* A bi-ventricular cardiac atlas built from 1000+ high resolution MR images of healthy subjects and an analysis of shape and motion. *Med. Image Anal.* **26**, 133–145 (2015).
43. Ware, J.S. *et al.* Shared genetic predisposition in peripartum and dilated cardiomyopathies. *N. Engl. J. Med.* **374**, 233–241 (2016).
44. Watkins, H. Tackling the Achilles' heel of genetic testing. *Sci. Transl. Med.* **7**, 270fs1 (2015).

ONLINE METHODS

Rat studies. Rat TTNtv models were generated by SAGE Laboratories using zinc-finger nuclease–mediated gene targeting. Rats were maintained on a F344 background. For the A-band (C terminus)-truncating variant (TTNtvA), 12 bp were deleted and 2 bp were inserted (TA) at 228,608–228,619 to introduce a stop codon in exon 303 (RefSeq NC_005102.3) corresponding to exon 327 in the human sequence. For the Z-disc (N terminus)-truncating mutation (TTNtvZ) was generated by deletion of exons 2–6 (5,286-bp deletion, coordinates 2,323–7,608) to introduce a frameshift. For details, see **Supplementary Figure 1**. Genotypes were detected by PCR, and products were confirmed by Sanger sequencing. Rat studies were conducted in accordance with the principles and procedures outlined in the National Institutes of Health Guide for the Care and Use of Laboratory Animals and were approved by the Institutional Animal Care and Use Committee (2013/SHS/844) at the Duke–National University of Singapore Medical School.

To enable allele-specific expression analyses with RNA–seq and Ribo–seq, we crossed wild-type, TTNtvA and TTNtvZ F344 rats with healthy BN rats. These F_1 rats were only used for sequencing experiments. The wild-type strain carried one non-truncated BN *Ttn* allele and one non-truncated F344 *Ttn* allele. The TTNtvA and TTNtvZ strains carried one truncated F344 *Ttn* allele and one non-truncated BN *Ttn* allele.

Patient and control cohorts and rare TTNtv burden testing. Data were collated from previously published case series[2–4], alongside a new cohort of 1,105 patients with DCM and 571 healthy controls. Overall, *TTN* sequencing was performed in a total of 2,495 cases and 61,834 reference samples. The case cohorts included 689 previously published probands[3], 241 previously published cases[2] (a UK cohort from this study, originally denoted DCM-B, was excluded because of overlap with the series from Roberts *et al.*), 156 probands referred to the Partners Healthcare Laboratory of Molecular Medicine for molecular diagnostics[45,46] and 304 probands similarly referred to the Oxford Medical Genetics Laboratory (OMGL), UK[46]. Further prospective unselected patients with a diagnosis of DCM, confirmed using cardiac imaging with reference to established cardiac MRI or echocardiographic diagnostic criteria as previously described[3], were recruited via the NIHR Royal Brompton Cardiovascular Biomedical Research Unit (n = 542), the German Center for Cardiovascular Research, Berlin (n = 386) and the National Heart Centre, Singapore (n = 177) and are reported here for the first time. These latter cohorts were sequenced on the Illumina MiSeq, Illumina NextSeq or Life Technologies SOLiD 5500xl platform after target enrichment using in-solution hybridization (Illumina Nextera[47] or Agilent SureSelect[3]), with analysis using standard pipelines as previously described[3]. The research studies were approved by a research ethics committee, and all participants gave written informed consent.

Informatics pipelines were used to define TTNtv as previously described[3]. TTNtv included frameshift, non-canonical stop and essential splice-site variation.

Reference samples comprised the ExAC (n = 60,706) database[11] (version 0.3, January 2015), alongside 557 controls from our previous studies[2,3] after exclusion of control cohorts that overlapped with ExAC and 571 unpublished controls recruited at the National Heart Centre, Singapore.

Rare variants that were predicted to truncate full-length *TTN* were included in analyses (variants were defined as rare if thy had an ExAC minor allele frequency (MAF) $<1 \times 10^{-4}$; variants were predicted to be truncating if they constituted a nonsense, frameshift insertion or deletion or disrupted a canonical splice donor/acceptor sequence; the *TTN* reference was the inferred complete meta-transcript LRG391_t1).

Variants were first grouped according to their location within the titin structure and expression of the exon in which they were found (PSI). We considered exons to be constitutive if they were spliced into at least 90% of the *TTN* transcripts present in the heart (PSI 90%). For each region, the prevalence of TTNtv in cases and controls were compared using the binomial test in R.

The constitutive *TTN* exons (plus 2-bp canonical splice sequences) were divided into 40 uniformly sized bins. For each bin, the total number of TTNtv alleles was compared in cases and controls, an odds ratio was computed and the etiological fraction (EF; the probability that an individual rare variant, found in a proband was responsible for the disease) was calculated using

$$\mathrm{EF} = \frac{\text{odds ratio} - 1}{\text{odds ratio}}$$

as previously described[46].

RNA–seq and Ribo–seq library preparation. To assess the translational status of wild-type and *Ttn*-mutant rats, ribosome profiling libraries were generated as previously described[15]. Briefly, ~70 mg of cardiac tissue was used for each animal and strain (wild-type, n = 4; TTNtvA, n = 3; TTNtvZ, n = 3) and subjected to cryolysis in 1 ml of lysis buffer (1× TruSeq Mammalian Polysome buffer (Illumina), 1% Triton X-100, 0.1% NP-40, 1 mM DTT, 10 U/ml DNase I and nuclease-free water) supplemented with 0.1 mg/ml cycloheximide (Sigma). Tissue was further homogenized using a 21-gauge syringe needle, incubated on ice for 10 min and centrifuged at 20,000g. 400 µl of lysate per sample was used to obtain ribosome footprints (RPFs) upon incubation with TruSeq Ribo Profile Nuclease (3 U per OD_{260}/ml of lysate). RPF purification was performed using MicroSpin S-400 columns (GE Healthcare) followed by phenol-chloroform RNA extraction. Mammalian rRNA was subsequently removed using the procedures described for the RiboZero Magnetic Gold kit (Epicentre). Ribosome footprints are expected to be 28–30 nt long. To recover fragments in this exact size window, purified fragments were resolved under denaturing PAGE. Following adaptor ligation, reverse transcription and a second denaturing PAGE purification, samples were circularized. Ribo–seq libraries were amplified by PCR (12 cycles) using the circularized products as template. PCR-amplified libraries were purified on native 8% polyacrylamide gels and quantified using the Qubit fluorometer. The quality and average fragment size of the libraries were instead assessed with the Bioanalyzer High-Sensitivity Assay (Agilent Technologies). To reduce technical biases, samples were barcoded and pooled to perform multiplex sequencing on the HiSeq 2000 platform (single-end, 50-bp sequencing chemistry).

To assess transcript abundance, stranded poly(A)$^+$ RNA–seq was performed following standard instructions from the manufacturer (TruSeq Stranded mRNA–seq Library Prep kit), using 1 µg of total RNA as input. Libraries were pooled and sequenced on a HiSeq 2000 instrument (paired-end, 100-bp sequencing chemistry).

Read mapping. We used Illumina CASAVA 1.8 software to demultiplex all reads and convert bcl files to fastq files. We then clipped adaptors from the Ribo–seq cDNA inserts using the FASTX-Toolkit (http://hannonlab.cshl.edu/fastx_toolkit/index.html). Adaptors were clipped using the command

```
fastx_clipper -a AGATCGGAAGAGCACACGTCT -l 20 -n -v -Q33 |
fastx_trimmer -Q33 -f 1
```

We then processed the RNA–seq reads in a similar manner and trimmed them to a length of 29 bp, the most abundant read length found in Ribo–seq, using the command

```
fastx_trimmer -l 29 -Q33
```

Trimming the RNA–seq data before mapping ensures that we can compare the two methodologies and draw conclusions regarding translational regulation. This step avoids differences in expression estimates that arise because of technical differences between the methods. We then removed mitochondrial RNA and rRNA sequences from all libraries using the Bowtie[48,49] with the command

```
bowtie -l 20 --un clean.fastq /abundant_sequences
input.fastq -S abundant.sam
```

Abundant sequences were stored in a Bowtie index derived from the fastq files for the rat mitochondrial genome and rRNA sequences annotated in the

doi:10.1038/ng.3719

Ensembl database[50]. Sequences that did not align (`clean.fastq`) were then further mapped to the genome using TopHat 2.0.13 (ref. 51) with the rn5 genome

```
tophat2 --read-realign-edit-dist 0 -p 6 -z0 -M -j
HiQual.juncs -G Rattus_norvegicus.Rnor_5.0.79_TTN.gtf rn5
R1.fastq
```

To improve the mapping of these short reads, we introduced splicing junctions as described previously[15]. We also supplied Ensembl[50] rat genome annotation v79 to the mapping pipeline. *Ttn* is not well annotated in rat, so we decided to lift over human *TTN* to the rat genome. We used the liftOver tool of the Galaxy[52,53] platform with standard parameters to transfer the *TTN* transcript model[3] to the rn5 genome. Split reads in RNA–seq data were used to confirm exon boundaries in rat. Titin regions and domains are shown as reported previously in human[3]. The Ensembl gene IDs corresponding to parts of titin were removed from the annotation and replaced with our custom titin annotation before the mapping step, which was then used for all analyses further downstream.

To analyze alternative splicing, we did not trim the RNA–seq reads but used the full-length 2 × 100-bp paired-end data to improve the estimation of splice-site usage in rat with the command

```
tophat2 --read-realign-edit-dist 0 -p 6 --no-cover-
age-search -M -j HiQual.juncs -G Rattus_norvegicus.
Rnor_5.0.79_TTN.gtf rn5 R1.fastq R2.fastq
```

Read periodicity. To determine the quality of the Ribo–seq data, we calculated the percentage of reads starting at a position that was indicative for ribosomes located on a codon of the ORF. We first selected 29-mers and then extracted the position of the A of the ATG start codon. This position is indicated by the location of the 5′ UTRs annotated by Ensembl[50] Biomart. Plotting the start positions of 29-mers in a window around the ATG codons of known genes showed a peak of read starts 12 bp upstream of the start codon. This is indicative for ribosomes located at the translation start site. Subsequently, read starts were preferentially located periodically every 3 bp, representing actively translating ribosomes reading the genetic message while synthesizing new protein. All libraries generated showed very high periodicity, with more than 90% of reads located in frame.

To determine whether the ribosomes localized to *Ttn* after the truncation in TTNtvZ rats are translating canonical titin sequence, we first determined the coding frame for each exon in wild-type rats. We then compared the percentage of reads located in this frame in wild-type and TTNtvZ rats and did not detect a difference across the locus. This indicates that ribosomes associated with the truncated titin isoforms are located in frame. We only determined periodicity in cardiac exons that were covered by at least ten read starts to avoid noise due to low coverage.

Gene expression analyses. To assess gene transcription and translation levels, we counted uniquely mapping reads that were unambiguously assigned to one gene with htseq-count using the command

```
htseq-count --stranded=no --type=CDS --quiet --
idattr=gene_id - Rattus_norvegicus.Rnor_5.0.79_
TTN.gtf
```

We only considered reads mapping to the coding sequence of genes annotated in Ensembl database v79 (ref. 50) for both the Ribo–seq and RNA–seq data sets. To detect genes differentially expressed between genotypes, we used the DESeq2 package[54] with standard parameters (false discovery rate (FDR) ≤ 0.05) for comparison of the two TTNtv models to wild-type rats. All genes that were detected in any of the comparisons are reported in the **Supplementary Figure 6** and **Supplementary Table 1**).

Gene and exon expression levels are given in RPKM. Reads overlapping a feature were normalized to the length of the feature and the number of uniquely mapping reads (that is, sequencing depth). Unlike read counts, these values can be used to compare RNA expression levels for different features within the same sample.

To assess allele-specific transcription and translation, we first identified all F344 SNPs on the BN background annotated by the rat genome database[55] that overlapped with the *Ttn* locus (http://rgd.mcw.edu/). We then counted the reads overlapping these positions and assigned them to either the BN or F344 allele depending on their sequence. Allele frequency across these positions corresponds to the ratio of *Ttn* transcripts originating from non-truncated *Ttn* (BN) and truncated *Ttn* (F344) in the TTNtv models.

The sum of the number of reads assigned to the BN or F344 allele was calculated for each rat, normalized by library size; these sums were then compared between wild-type and TTNtvA or TTNtvZ rats. To avoid BN- or F344-specific differences in *Ttn* expression disturbing signal, we normalized the expression levels of both alleles to the levels in wild-type rats.

To assess protein synthesis levels for full-length titin, we considered all Ribo–seq reads that we could assign to regions exclusive to the non-truncated alleles in TTNtv rats and compared counts to those for wild-type rats. In TTNtvA rats, all Ribo–seq reads located after the premature stop codon are derived from the BN allele. This is indicated by the complete absence of F344 SNPs in the data due to efficient stop of translation after the premature stop codon. The proximal truncation in TTNtvZ rats does not completely stop translation, and Ribo–seq reads downstream of the premature stop codon are not necessarily representative of expression of full-length titin. These reads partly derive from isoforms with alternative N termini that are not truncated by the TTNtvZ mutation. Anticipating this, we chose to generate a stop by introducing a large deletion that encompassed several exons. These exons (exons 3–5) are only present in the BN allele, and reads mapping to this region are thus indicative of expression of full-length titin in the absence of a truncation in TTNtvZ rats.

We also assessed the translation of each exonic part of *Ttn* across all rat models. We only considered exons with an expression level of RPKM >1 in rat heart ($n = 237$). FPKM values from all three replicates for each TTNtv model were compared to those for wild-type rats, and outliers were removed (ROUT $Q = 1\%$). We then calculated the average ratio for each exon across all biological replicates and performed second-order polynomial smoothing using ten neighbors to generate the average. Smoothing was required to visualize a trend of translation rates in comparison to healthy rats across the entire *Ttn* locus.

To assess allele frequency in the RNA–seq and Ribo–seq data, we required the location of each F344 SNP ($n = 121$) to be covered by at least two reads on average across all rats.

Detection of alternative transcription start site expression in human heart. To identify transcription start sites in *TTN*, two sources of data were used. First, CAGE data from heart tissue in the FANTOM5 consortium data set[13] were used to identify the location of active transcription start sites. Second, ChIP–seq data were used from heart tissue for two histone marks associated with the presence of an active promoter, namely H3K4me3 and H3K9ac, in the Epigenomics Roadmap data set[16]. Specifically, the FANTOM5 heart samples were CNhs11758, CNhs11757, CNhs10621, CNhs10653, CNhs12855, CNhs12856 and CNhs12857, for which data were downloaded using CAGEr[56]. These data were then processed using CAGEr (standard parameters) to identify transcription start sites by first normalizing the tag counts using a power law and then clustering the reads to find CAGE peaks that corresponded to active transcription start sties. This approach identified three transcription start sites within the *TTN* region. To further validate these sites, narrow H3K4me3 peaks from sample E095 (adult heart left ventricle) and narrow H3K9ac peaks and narrow H3K4me3 peaks from sample E083 (fetal heart) were downloaded from the Epigenomics Roadmap data portal and overlaid onto *TTN*. This showed corresponding histone modifications for two of the three transcription start sites identified using CAGEr. All of these data sets were then plotted using circlize[57].

Percent spliced in. To assess splicing of *Ttn* in TTNtv hearts, we calculated the PSI ratio for all exons in *TTN* across species. PSI is a measure of how efficiently an exon is spliced into the final isoform population of a gene. First, we generated an exonic matrix based on our custom *Ttn* annotation using the prepare_annotation tool[58]. Then, we executed the PSI.sh[17] script to calculate PSI ratios with the following parameters:

```
PSI.sh StartPSIStrictFilter TTN_exonic.gtf 100
accepted_hits.bam junctions.bed PSI_result
```

We slightly altered the script and included a more stringent filter for read exclusion to avoid mapping artifacts from split alignments. Every exclusion read was required to start and end at a known exon boundary to be considered in the final PSI calculation (StrictFilter). We also calculated PSI values for human cardiac DCM samples with and without TTNtv for previously reported patients[3]. We then compared patterns of *TTN* isoform regulation between patients with DCM carrying truncating variants in *TTN* and those who did not carry these variants, by means of ΔPSI: mean(PSI(DCM TTNtv)) – mean(PSI(DCM controls)).

Exons with a PSI value in heart of at least 15% are considered cardiac and at least 90% are considered constitutive exons throughout the manuscript.

Pathway analysis. To better understand the effects of TTNtv on the genome-wide molecular landscape of the heart, we identified over-represented pathways among differentially transcribed and translated genes. We used counts normalized by DESeq2 (ref. 54) and performed a KEGG[23] pathway enrichment analysis with GAGE[22]

```
res <- gage(counts,gsets = kegg.gs,ref = 4:7,samp =
1:3,compare = "unpaired")
```

where columns 4–7 presented normalized counts for wild-type rats and columns 1–3 presented counts from TTNtv rats. Ensembl IDs were converted to Entrez IDs before this analysis using Biomart[50]. GAGR does not rely on a list of significant differential genes but instead performs a statistical test of whether the fold changes in a certain pathway are more different between groups than expected. This enabled us to detect affected pathways in comparison of groups with great sensitivity.

Rat magnetic resonance imaging. Rats (13 to 16 months old) were anaesthetized using 1–3% isoflurane and maintained at 0.5–1.5% isoflurane during the imaging session. Heart rate, blood oxygen saturation, respiratory rate, temperature and ECG were monitored (SA Instruments). Imaging was performed on a 7T ClinScan small-animal MRI machine (Bruker Ettlingen) equipped with a rat cardiac array surface coil. 2D cine gradient echo sequences were acquired in long-axis, four-chamber and short-axis views of the left ventricle[59]. Left ventricle chamber volume was quantified using Segment v2.0 R4377 software[60] (Medviso), and left ventricle wall parameters were measured as previously described[61].

Rat echocardiography. Four- to 8-month-old rats were initially anesthetized with 2–2.5% isoflurane and maintained at 1.6–2.0% isoflurane during image acquisition. Transthoracic echocardiographic measurements were performed on a Vevo 2100 system with the MS250 linear array transducer, 13–24 MHz (VisualSonics). Standard 2D and M-mode short-axis views at the mid-papillary muscle level were acquired, and an average of ten cardiac cycles were stored in cine loops for subsequent offline analysis using the same system[62,63].

***Ex vivo* Langendorff studies.** Rats (13–16 weeks old) were anesthetized with ketamine (80 mg/kg) and xylazine (10 mg/kg) via intraperitoneal injection. Heparin (1,000 U) was administered subcutaneously, and the heart was excised and perfused with modified Krebs–Henseleit buffer solution in a retrograde fashion on a Langendorff apparatus[64] (ADInstruments). An incision was made to the left atrium, and a fluid-filled latex balloon was placed in the left ventricular cavity. End diastolic pressure was set at between 5 and 10 mm Hg for all hearts for baseline measurements by adjustment of the volume of buffer in the latex balloon. Hearts were paced at 300 beats/min. To mimic volume overload, the volume of buffer in the balloon in the left ventricular cavity was progressively increased by 10 µl every 5 min up to a final incremental volume of 40 µl. Myocardial contractility (dP/dt_{max}) and relaxation rates (dP/dt_{min}) were derived from left ventricular developed pressure (LVDevP) using the MLT844 physiological pressure transducer. Data were acquired and analyzed using LabchartPro software (ADInstruments).

Metabolomic analysis. Rat hearts were snap frozen in liquid nitrogen and stored at −80 °C before analysis. Acylcarnitine profiling was performed as described[65]. Briefly, 50 to 100 mg of tissue was homogenized in 50% acetonitrile, 0.3% formic acid. Tissue homogenates were extracted using methanol and derivatized using 3 M HCl in methanol (Sigma-Aldrich), dried and reconstituted in methanol for analysis by LC–MS using the Agilent 6430 Triple-Quadrupole LC/MS system (Agilent Technologies). A 2-µl sample was injected at 0.4 ml/min with an 80:20 ratio of methanol to water as the mobile phase. Raw data analysis was performed on Agilent MassHunter Workstation B.06.00 software.

CE–TOFMS (capillary electrophoresis and time-of-flight mass spectrometry) was performed to quantify glycolytic intermediates, energy substrates and amino acids. Heart tissue was mixed in 50% acetonitrile in water containing internal standards (40 µM for cation measurement and 10 µM for anion measurement) and homogenized (1,500 r.p.m. for 120 s, five times) before addition of 50% acetonitrile in water. The supernatant was then passed through a filter with a 5-kDa cutoff (Human Metabolome Technologies) to remove macromolecules, and the filtrate was concentrated by centrifugation and resuspended in ultra-pure water before metabolite measurement. Compounds were analyzed using the Agilent capillary electrophoresis system equipped with an Agilent 6210 TOFMS, a 1100 isocratic HPLC pump, a G1603A CE–MS adaptor kit and a G1607A CE and electrospray ionization–mass spectrometry (ESI–MS) sprayer kit (Agilent Technologies). The system was controlled using G2201AA ChemStation software (Agilent Technologies).

Cationic metabolites were analyzed using a fused silica capillary (50-µm internal diameter × 80-cm length) with Cation Buffer solution (H3301-1001, Human Metabolome Technologies). The samples were injected at a pressure of 50 mbar for 10 s, and the positive applied voltage was 27 kV. ESI–MS was conducted in a positive-ion mode with the capillary voltage set at 4,000 V. Samples were scanned from 50 to 1,000 m/z (ref. 66). Anionic metabolites were analyzed using a fused silica capillary (50-µm internal diameter × 80-cm length) with Anion Buffer solution (H3302-1021, Human Metabolome Technologies). Samples were injected at a pressure of 50 mbar for 25 s, and the positive applied voltage was 30 kV. ESI–MS was conducted in a negative-ion mode with the capillary voltage set at 3,500 V. Samples were scanned from 50 to 1,000 m/z (ref. 67).

Raw data obtained by CE–TOFMS were processed using automatic integration software (MasterHands v. 2.17.1.11, Keio University) to obtain peak information[68]. Peak area was converted to relative peak area, and the peak detection limit was determined on the basis of the signal/noise ratio: $S/N = 3$. Putative metabolites were then assigned from the HMT standard library and known–unknown peak library on the basis of m/z values and migration time. Absolute quantification was obtained by single-point (100 µM) calibration and further normalized by sample weight.

Glucose-6-phosphate assays. Rat hearts were snap frozen in liquid nitrogen and stored at −80 °C before analysis. Heart tissue was homogenized in ice-cold PBS, and samples were deproteinized according to the manufacturer's instructions (ab204708, Abcam). Deproteinized samples were added to duplicate wells of a 96-well plate, and G6P content was determined according to the manufacturer's instructions (ab83426, Abcam).

Titin protein quantification. SDS–PAGE was performed on 2.5% polyacrylamide/1% agarose gels, and total protein was visualized by Coomassie blue staining. Titin protein was visualized at approximately 3 MDa, and its levels were normalized to those of MyHC (205 KDa) as a loading control. For immunoblotting quantification, total protein was separated on 1.8% polyacrylamide/1% agarose gels, transferred to PVDF membrane and probed with T12 antibody against the N terminus of titin and Novex3 as previously described[9].

Immunoblotting. Rat left ventricle tissue was homogenized in primary lysis buffer (50 mM sodium phosphate, pH 7.4, 150 mM NaCl and 1% Triton X-100 with protease and phosphatase inhibitor cocktail (Sigma)) and then centrifuged. The supernatant was collected, and a secondary extraction was performed on the pellet containing nuclear, structural and membrane proteins using secondary lysis buffer (1% SDS, 5 mM EDTA, 10 mM DTT,

doi:10.1038/ng.3719

15 U/ml DNase I, and protease and phosphatase inhibitors). The primary and secondary extracts were combined, and protein concentration was determined by BCA protein assay (Pierce, Thermo Scientific). Equal amounts of protein were separated by SDS–PAGE, transferred to PVDF membranes and probed with antibody to mTOR pSer2448 (2971), 4EBP1 pThr37/Thr46 (2855), S6K pThr389 (9205), mTOR (2972), S6K (2708), 4EBP1 (9644), GAPDH (2118) or β-tubulin (2146) from Cell Signaling Technology. All antibodies were diluted at 1:1,000.

Healthy volunteer magnetic resonance imaging. Healthy volunteers without self-reported cardiovascular disease or a family history of disease were recruited prospectively via advertisement to the UK Digital Heart Project (https://digital-heart.org/) at the MRC-CSC, Imperial College, London[69]. The study was approved by a research ethics committee, and all participants gave written informed consent.

Conventional 2D and high-resolution 3D cine balanced steady-state free precession (b-SSFP) CMR imaging were performed on a 1.5T Philips Achieva system (Best)[41]. Analysis of the CMR scans was carried out by two experienced cardiologists, blinded to genotyping data, using commercially available semiautomated software (CMRtools, Cardiovascular Imaging Solutions). Measurements followed standard methodology[70,71], with papillary muscles included in the left ventricular mass and valve position tracked in the long-axis images. 3D CMR data were segmented and co-registered to provide a model of phenotypic variation in the population[42].

Statistical analysis. GraphPad Prism 6 software was used for statistical analysis. For two factors, trend testing was performed with two-way ANOVA. Comparison of two means was performed by two-tailed *t* test. When several conditions were each compared to one reference condition, we performed Dunnett's test to correct for multiple testing. Data are reported as means ± s.e.m. or s.d. as described[42], with significance levels of $*P < 0.05$, $**P < 0.01$ and $***P < 0.001$. Using RStudio Server version 0.98, standard linear regressions were performed to evaluate the relationship between TTNtv genotype and cardiovascular phenotypes, as previously described[3]. Multivariate models were generated using known clinical covariates and optimized to minimize the Bayesian information criterion. The relationships between morphological parameters and *TTN* genotype were assessed by ANOVA between nested linear models. To test for position-independent association of TTNtv across *TTN*, we performed binomial tests. 3D phenotypic regression modeling applied threshold-free cluster enhancement and permutation testing to derive the *P* values associated with each regression coefficient following adjustment to control the FDR[72,73].

Data availability. The RNA–seq and Ribo–seq data used in the manuscript can be obtained from the European Nucleotide Archive (ENA) under accession ERP015402.

45. Pugh, T.J. *et al.* The landscape of genetic variation in dilated cardiomyopathy as surveyed by clinical DNA sequencing. *Genet. Med.* **16**, 601–608 (2014).
46. Walsh, R. *et al.* Reassessment of Mendelian gene pathogenicity using 7,855 cardiomyopathy cases and 60,706 reference samples. *Genet. Med.* http://dx.doi.org/10.1038/gim.2016.90 (2016).
47. Pua, C.J. *et al.* Development of a comprehensive sequencing assay for inherited cardiac condition genes. *J. Cardiovasc. Transl. Res.* **9**, 3–11 (2016).
48. Langmead, B., Trapnell, C., Pop, M. & Salzberg, S.L. Ultrafast and memory-efficient alignment of short DNA sequences to the human genome. *Genome Biol.* **10**, R25 (2009).
49. Langmead, B. & Salzberg, S.L. Fast gapped-read alignment with Bowtie 2. *Nat. Methods* **9**, 357–359 (2012).
50. Cunningham, F. *et al.* Ensembl 2015. *Nucleic Acids Res.* **43**, D662–D669 (2015).
51. Kim, D. *et al.* TopHat2: accurate alignment of transcriptomes in the presence of insertions, deletions and gene fusions. *Genome Biol.* **14**, R36 (2013).
52. Goecks, J., Nekrutenko, A., Taylor, J. & Team, T. Galaxy: a comprehensive approach for supporting accessible, reproducible, and transparent computational research in the life sciences. *Genome Biol.* **11**, R86 (2010).
53. Giardine, B. *et al.* Galaxy: a platform for interactive large-scale genome analysis. *Genome Res.* **15**, 1451–1455 (2005).
54. Love, M.I., Huber, W. & Anders, S. Moderated estimation of fold change and dispersion for RNA–seq data with DESeq2. *Genome Biol.* **15**, 550 (2014).
55. Shimoyama, M. *et al.* The Rat Genome Database 2015: genomic, phenotypic and environmental variations and disease. *Nucleic Acids Res.* **43**, D743–D750 (2015).
56. Haberle, V., Forrest, A.R., Hayashizaki, Y., Carninci, P. & Lenhard, B. CAGEr: precise TSS data retrieval and high-resolution promoterome mining for integrative analyses. *Nucleic Acids Res.* **43**, e51 (2015).
57. Gu, Z., Gu, L., Eils, R., Schlesner, M. & Brors, B. circlize implements and enhances circular visualization in R. *Bioinformatics* **30**, 2811–2812 (2014).
58. Anders, S., Reyes, A. & Huber, W. Detecting differential usage of exons from RNA–seq data. *Genome Res.* **22**, 2008–2017 (2012).
59. Price, A.N. *et al.* Cardiovascular magnetic resonance imaging in experimental models. *Open Cardiovasc. Med. J.* **4**, 278–292 (2010).
60. Heiberg, E. *et al.* Design and validation of Segment—freely available software for cardiovascular image analysis. *BMC Med. Imaging* **10**, 1 (2010).
61. Ross, A.J. *et al.* Serial MRI evaluation of cardiac structure and function in mice after reperfused myocardial infarction. *Magn. Reson. Med.* **47**, 1158–1168 (2002).
62. Tortoledo, F.A., Quinones, M.A., Fernandez, G.C., Waggoner, A.D. & Winters, W.L. Jr. Quantification of left ventricular volumes by two-dimensional echocardiography: a simplified and accurate approach. *Circulation* **67**, 579–584 (1983).
63. Sahn, D.J., DeMaria, A., Kisslo, J. & Weyman, A. Recommendations regarding quantitation in M-mode echocardiography: results of a survey of echocardiographic measurements. *Circulation* **58**, 1072–1083 (1978).
64. Sutherland, F.J. & Hearse, D.J. The isolated blood and perfusion fluid perfused heart. *Pharmacol. Res.* **41**, 613–627 (2000).
65. Muoio, D.M. *et al.* Muscle-specific deletion of carnitine acetyltransferase compromises glucose tolerance and metabolic flexibility. *Cell Metab.* **15**, 764–777 (2012).
66. Soga, T. & Heiger, D.N. Amino acid analysis by capillary electrophoresis electrospray ionization mass spectrometry. *Anal. Chem.* **72**, 1236–1241 (2000).
67. Soga, T. *et al.* Simultaneous determination of anionic intermediates for *Bacillus subtilis* metabolic pathways by capillary electrophoresis electrospray ionization mass spectrometry. *Anal. Chem.* **74**, 2233–2239 (2002).
68. Sugimoto, M. *et al.* Differential metabolomics software for capillary electrophoresis–mass spectrometry data analysis. *Metabolomics* **6**, 27–41 (2010).
69. de Marvao, A. *et al.* Precursors of hypertensive heart phenotype develop in healthy adults: a high-resolution 3D MRI study. *JACC Cardiovasc. Imaging* **8**, 1260–1269 (2015).
70. Bellenger, N.G., Grothues, F., Smith, G.C. & Pennell, D.J. Quantification of right and left ventricular function by cardiovascular magnetic resonance. *Herz* **25**, 392–399 (2000).
71. Grothues, F. *et al.* Comparison of interstudy reproducibility of cardiovascular magnetic resonance with two-dimensional echocardiography in normal subjects and in patients with heart failure or left ventricular hypertrophy. *Am. J. Cardiol.* **90**, 29–34 (2002).
72. Smith, S.M. & Nichols, T.E. Threshold-free cluster enhancement: addressing problems of smoothing, threshold dependence and localisation in cluster inference. *Neuroimage* **44**, 83–98 (2009).
73. Benjamini, Y. & Hochberg, Y. Controlling the false discovery rate: a practical and powerful approach to multiple testing. *J. R. Stat. Soc. B* **57**, 289–300 (1995).